Research Article

Journal of PeptideScience

Received: 9 August 2011 Revised: 2 November 2011 Accepted: 1 December 2011 Published online in Wiley Online Library: 17 January 2012

(wileyonlinelibrary.com) DOI 10.1002/psc.2391

Hexafluoroisopropanol induces self-assembly of β-amyloid peptides into highly ordered nanostructures

Sanjai Kumar Pachahara,[§] Nitin Chaudhary,[§‡] Chilukuri Subbalakshmi and Ramakrishnan Nagaraj*

Deposition of insoluble fibrillar aggregates of β-amyloid (Aβ) peptides in the brain is a hallmark of Alzheimer's disease. Apart from forming fibrils, these peptides also exist as soluble aggregates. Fibrillar and a variety of nonfibrillar aggregates of Aβ have also been obtained *in vitro*. Hexafluoroisopropanol (HFIP) has been widely used to dissolve Aβ and other amyloidogenic peptides. In this study, we show that the dissolution of Aβ40, 42, and 43 in HFIP followed by drying results in highly ordered aggregates. Although α-helical conformation is observed, it is not stable for prolonged periods. Drying after prolonged incubation of Aβ40, 42, and 43 peptides in HFIP leads to structural transition from α-helical to β-conformation. The peptides form short fibrous aggregates that further assemble giving rise to highly ordered ring-like structures. Aβ16–22, a highly amyloidogenic peptide stretch from Aβ, also formed very similar rings when dissolved in HFIP and dried. HFIP could not induce α-helical conformation in Aβ16–22, and rings were obtained from freshly dissolved peptide. The rings formed by Aβ40, 42, 43, and Aβ16–22 are composed of the peptides in β-conformation and cause enhancement in thioflavin T fluorescence, suggesting that the molecular architecture of these structures is amyloid-like. Our results clearly indicate that dissolution of Aβ40, 42 and 43 and the amyloidogenic fragment Aβ16–22 in HFIP results in the formation of annular amyloid-like structures. Copyright © 2012 European Peptide Society and John Wiley & Sons, Ltd.

Keywords: amyloid fibrils; self-assembly; ring-like structures; fluorinated alcohol

Introduction

β-amyloid (Aβ) peptides composed of 40–43 residues are the constituents of amyloid fibrils that are responsible for Alzheimer's disease [1,2]. In human brain, Aβ40 is the predominant alloform followed by Aβ42 [3]. Aβ42, although constitutes only 10% of total Aβ, has higher tendency to form amyloid fibrils and is therefore considered to be pathologically relevant [3,4]. Aβ43 also forms fibrils that could be clinically important [5]. The mature fibrils formed by these peptides are highly insoluble and need treatment with denaturants or strong acids or bases for solubilization [6,7]. Sonication is also employed to break up the Aβ aggregates [8,9]. Synthetic and recombinant Aβ42 peptides also form fibrils rapidly. The recombinant peptide was observed to aggregate more readily and was more neurotoxic than the synthetic one [10]. The structures of the aggregates are indistinguishable from those obtained from the pathological samples. Organic solvents, particularly trifluoroethanol (TFE) and hexafluoroisopropanol (HFIP), have been used intensively to dissolve peptides that tend to aggregate [11–14]. These solvents have also been used intensively to dissolve amyloid-forming peptides in order to have stock solutions in which peptides are monomeric [12,15]. Dissolution of Aβ peptides in HFIP followed by immediate drying has been one of the methods to make monomeric preparations of Aβ. In some cases, the dissolved Aβ peptides are stored for prolonged periods [16,17]. The ability of these solvents to favor or promote helical conformation is presumed to be the reason for their excellent solubilizing properties. We have shown that dissolution of short amyloid-forming peptides in TFE and HFIP can result in the formation of ring-like structures in addition to linear structures [18,19]. In aqueous solutions, Aβ40, 42, and 43 (denoted hereafter as Aβ40–43) form fibrillar structures with morphology depending on the aggregation conditions. However, oligomers of different sizes are also observed. The dynamic aspect of fibrillar structures is evident from a recent report that indicates molecular recycling of Aβ40 and Aβ42 within the fibril populations [20]. The formation of spherulites has also been observed *in vitro* with Aβ peptides from aqueous solutions on chemically modified quartz surface. These structures stain with thioflavin T (ThT) indicating their amyloid nature [21]. The spherulites have also been obtained in solution near physiological condition, and these spherulites are very similar to those formed *in vivo* and exhibit a maltese cross pattern [22]. Spherical assemblies of Aβ, also known as amylospheroids, have been inferred from fluorescence correlation spectroscopic studies [23]. The segment 16–20, that forms the core of the Aβ fibrils, is not involved in amylospheroid formation [23]. A variety of amyloid structures observed for Aβ peptides arise from aqueous

* *Correspondence to: Ramakrishnan Nagaraj, Council of Scientific and Industrial Research, Centre for Cellular and Molecular Biology, Uppal Road, Hyderabad 500 007, India. E-mail: nraj@ccmb.res.in*

‡ *Current address: Department of Biotechnology, Indian Institute of Technology Guwahati, Guwahati, 781 039, Assam, India*

§ *These authors have contributed equally to this work.*

Council of Scientific and Industrial Research, Centre for Cellular and Molecular Biology, Uppal Road, Hyderabad 500 007, India

solutions. Because Aβ40–43 peptides dissolve well in HFIP, we have examined the structures of these peptides from HFIP solution. We also examined the structures of Aβ16–22 that has the ability to form fibrils or nanotubes, depending on the pH, from aqueous solutions [24]. We have observed that highly ordered superstructures are formed by the Aβ peptides from HFIP solutions.

Materials and Methods

Peptide Solutions

The peptides Aβ40, Aβ42, and Aβ43 were purchased from Peptides International (Peptide Institute, Inc., Osaka, Japan) in the trifluoroacetate form. Identities of the peptides were confirmed by matrix-assisted laser desorption/ionization time-of-flight mass spectrometry. HFIP (200 μl) was added to the vials having lyophilized peptides. The concentrations of the peptides were estimated by diluting the peptides in water and recording absorption at 280 nm. Molar absorption coefficient of 1280 M^{-1} cm^{-1} at 280 nm was used to calculate the concentrations. The concentrations of Aβ40, Aβ42, and Aβ43 were 1.8 mM, 0.77 mM, and 0.83 mM, respectively. Aβ16–22 (Ac-KLVFFAE-am) was synthesized, purified, and characterized as described earlier [25]. The peptide was dissolved in HFIP to obtain 1 mM solution. Concentration was estimated by diluting the peptide in water and recording absorption at 254 nm. Molar absorption coefficient of 286 M^{-1} cm^{-1} at 254 nm was used to determine the concentration. The peptide solutions were stored at room temperature during the course of study.

Atomic Force Microscopy (AFM)

Peptides (1 μl) were deposited on freshly peeled mica surfaces and air dried before imaging. The images were acquired using tapping mode AFM (Multimode, Digital Instruments, Santa Barbara, CA, USA). A silicon probe was oscillated at 190–200 KHz and images were collected at an optimized scan rate. Analysis was carried out using Nanoscope (R) III 5.30 r1 software (Digital Instruments, Santa Barbara, CA, USA). All the images are second-order flattened and presented in the height mode. Height analysis was performed using 'Section' tool present in the Nanoscope software.

Scanning Electron Microscopy (SEM)

The peptides (2 μl) were deposited on glass coverslips from stock solutions prepared in HFIP and dried. The dried samples were sputter coated with gold using Polaron SC7620 Sputter Coater (Quorum Technologies Ltd., UK). SEM imaging of the gold-coated peptide samples was carried out on a Hitachi S-3400 N scanning electron microscope (Hitachi, Tokyo, Japan) at 5 or 10 kV.

Circular Dichroism (CD) Spectroscopy

Far-UV CD spectra of the peptides were recorded on Jasco J-815 spectropolarimeter (Jasco, Tokyo, Japan). Aβ40–43 peptides were diluted to 10 μM, whereas Aβ16–22 was diluted to 100 μM concentration into HFIP. The spectra were recorded in 0.1 cm path length cell by using a step size of 0.2 nm, band width of 1 nm, and scan rate of 100 nm min^{-1}. The spectra were recorded by averaging eight scans and corrected by subtracting the HFIP spectrum. Mean residue ellipticity ($[\theta]_{MRE}$) was calculated using the formula: $[\theta]_{MRE} = (M_r \times \theta_{mdeg})/(100 \times l \times c)$, where M_r = mean residue weight, θ_{mdeg} = ellipticity in millidegrees, l = path length in decimeter, and c = peptide concentration in mg ml^{-1}.

Fourier Transform Infrared (FTIR) Spectroscopy

FTIR spectra were recorded on a Bruker Alpha-E spectrometer (Bruker Optik GmbH, Ettlingen, Germany) with Eco attenuated total reflection (ATR) single reflection ATR sampling module equipped with ZnSe ATR crystal. Peptides were spread out and dried as films on ZnSe crystal and ATR-FTIR spectra were recorded. Each spectrum is the average of 64 FTIR spectra at a resolution of 4 cm^{-1}. All the spectra were normalized to the scale of zero to one arbitrary absorbance unit to facilitate easy comparison.

Thioflavin T (ThT) Fluorescence Microscopy

Peptide solutions (2 μl from stock solutions) were spread and dried as films on a glass coverslip. ThT solution (10 μl of 10 μM in deionized water) was layered on the dried peptide film. Fluorescence images were recorded on Zeiss Axiovert 200 microscope (Carl Zeiss, Oberkochen, Germany). Filter set with 450/50 nm excitation and 510/50 nm emission was used. The images were pseudocolored.

Results

Atomic Force Microscopy (AFM) Imaging

AFM images were recorded after drying the peptide solutions in HFIP on freshly peeled mica surfaces. Figure 1 shows the imaging

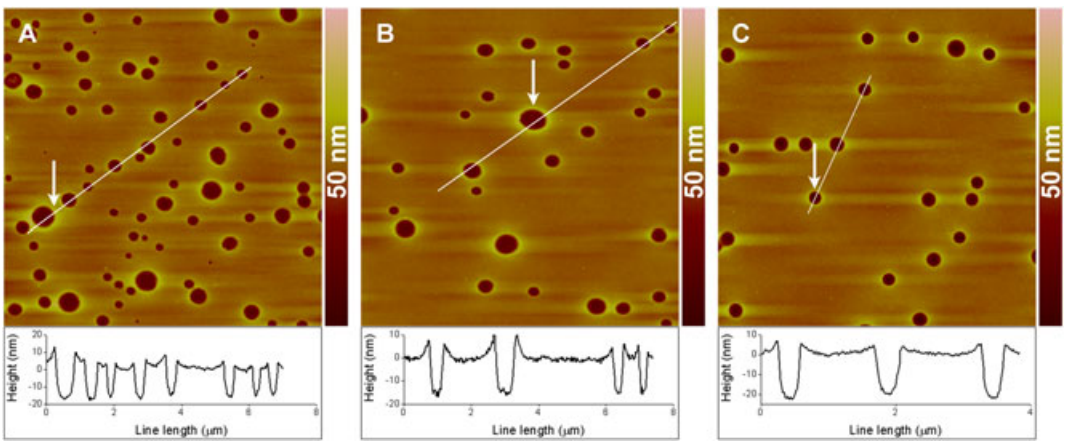

Figure 1. AFM images of freshly dissolved Aβ peptides when dried from HFIP: (A) Aβ40; (B) Aβ42; and (C) Aβ43. Arrows are described in the AFM imaging section. Each panel is 4 μm × 4 μm in dimensions.

Journal of PeptideScience

of Aβ40 (panel A), Aβ42 (panel B), and Aβ43 (panel C) samples after drying the freshly prepared solutions on mica. The peptides appear to be deposited as porous sheets. The height profiles shown below the individual panels were drawn for the white lines on the panels. Assuming that the pores completely span the peptide sheets, the thickness of the sheets could be measured using pore depths. The peptide sheets are not homogeneous and vary between ~10–20 nm for Aβ40 (panel A) and Aβ42 (panel B), and ~20 nm for Aβ43 (panel C). The boundaries for many of the pores are thicker than the background peptide layer giving them ring-like appearance (indicated by arrows). The height profiles indicate that the pores with ring-like appearance have ~2–4 nm higher thickness as compared with the background peptide sheets (indicated by arrows). As the entire area scanned was covered with the peptide, AFM images were recorded from the solutions that were tenfold diluted in the HFIP prior to layering on the mica surface (Figure 2). Panels A, B, and C represent the images recorded from tenfold diluted Aβ40, Aβ42, and Aβ43 samples, respectively. All the three peptides show ring-like structures. The diameters of the Aβ40 rings lie between 300 and 400 nm, and the thickness of the rings is ~1.8–4 nm (panel A). The thickness of the Aβ42 rings is similar to the Aβ40 rings (~1.8–4 nm), but the rings have two types of populations in terms of their diameters; large rings have diameters ~400–550 nm, whereas smaller rings are ~150 nm in diameter (panel B). The rings formed by Aβ43 are ~550–600 nm in diameter and approximately twofold thicker (~4–9 nm thick) as compared with those formed by Aβ40 and Aβ42. Fibers ~2 nm in diameter have been shown by AFM for Aβ42 and are suggested to be the single protofilament structure, that is structure with single cross-β unit [26–28]. The ring-like structures observed for Aβ appear to be arising from circularization of these protofilaments. Stacking of two protofilaments would result in the rings ~4 nm thick, as observed for Aβ40 and Aβ42 (panels A and B). The thicker rings observed for Aβ43 are likely to arise from stacking of more than two such protofilaments (panel C).

The peptide samples were aged at room temperature and AFM imaging was performed on these aged peptide samples (Figure 3). Panels A, B, and C represent images recorded from 4-month-old Aβ40, Aβ42, and Aβ43 samples, respectively. Long incubation at room temperature clearly results in thick rings as compared with the rings obtained from freshly prepared solutions (Figure 1). The rings formed by Aβ40 are 300–400 nm in diameter and ~8–15 nm in thickness. The Aβ42 ring shown in panel B is ~40–80 nm in thickness and ~320–350 nm in diameter when measured using section lines in different directions (one such section line shows the height profile below the image). The Aβ43 ring shown in panel

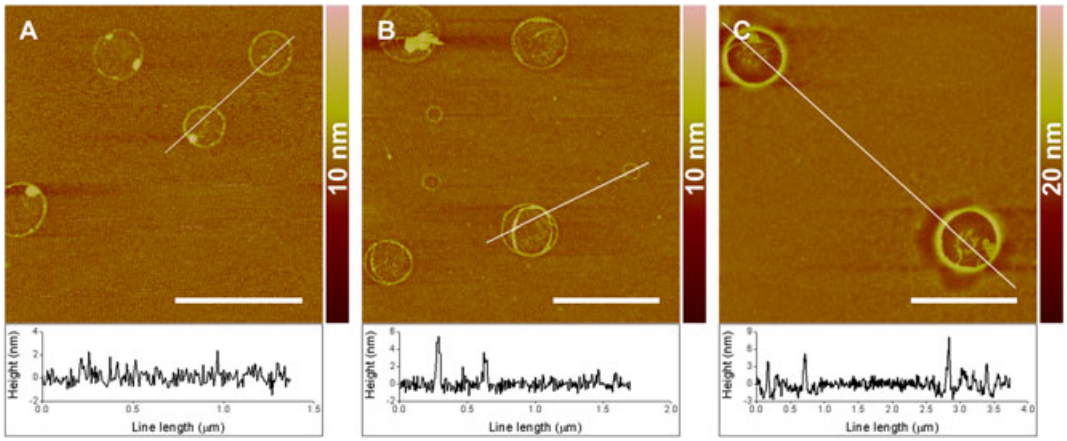

Figure 2. AFM images of freshly dissolved Aβ peptides that were tenfold diluted in HFIP prior to drying on mica: (A) Aβ40; (B) Aβ42; and (C) Aβ43. Scale bars represent 1 μm.

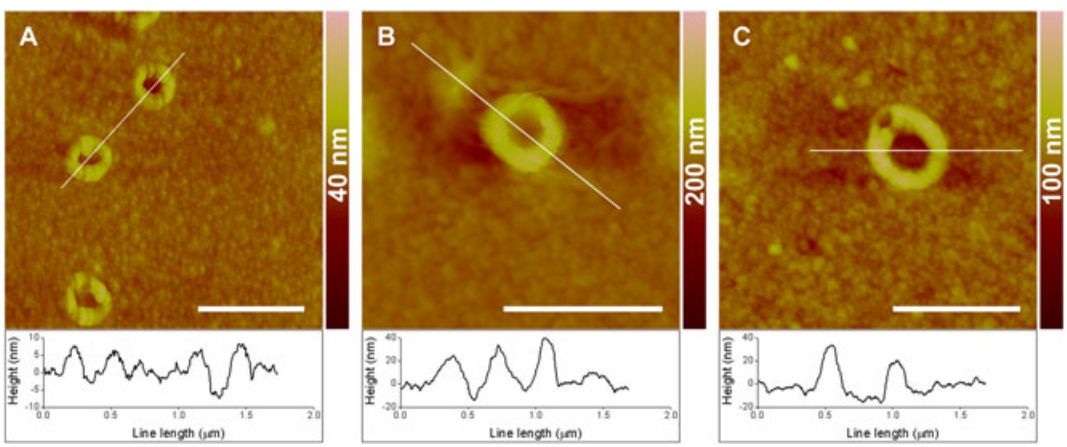

Figure 3. AFM images of 4-month-old Aβ peptides when dried from HFIP: (A) Aβ40; (B) Aβ42; and (C) Aβ43. Scale bars represent 1 μm.

C is ~30–50 nm in thickness and ~450–500 nm in diameter. Apart from the rings, spherical oligomers are also present covering the entire mica surface. The peptide solutions were tenfold diluted in HFIP and immediately deposited and dried on mica. Figure 4 shows the images recorded from these freshly diluted 4-month-old peptide solutions. Short fibrous aggregates as well as ring-like structures were observed for all the three peptides. Panel A shows the image recorded for Aβ40. The thickness of the short Aβ40 fibers ranges from very thin (~2 nm, indicated by dashed black arrows) to that characteristic of mature amyloid fibrils (up to 12 nm thick, indicated by solid black arrows). Thick fibers have tapered ends and appear to arise from the lateral assembly of thinner fibers. Unlike classical amyloid fibrils that are several micrometers long, the isolated Aβ40 fibers are very short (<500 nm in length). The thick fibers appear to arrange in circular fashion giving rise to the ring-like structures ~300–500 nm in diameter (indicated by white arrows). This suggests lateral as well as end-to-end assembly of short fibers giving rise to the rings. Aβ42 also forms short fibrous aggregates (panel B). Longer fibers (up to 2 μm in length) that appear to arise from lateral and end-to-end joining of the short fibers are also present (panel B, indicated by arrow). The rings formed are ~250–350 nm in diameter. Aβ43 also, like other two peptides, forms fibrillar structures that organize into ring-like structures ~200–250 nm in diameter (panel C, indicated by arrows). Apart from rings, Aβ43 also forms globular aggregates of varying diameter (100–180 nm) and height (20–50 nm). Aβ42 and Aβ43 form rings with diameters <400 nm, whereas rings obtained from freshly dissolved solutions were >400 nm in diameter. This decrease in the diameter of the rings can be attributed to the formation of closed rings without much of the loosely organized fibrils. Aβ42 and Aβ43 are more amyloidogenic as compared with Aβ40 and appear to pack more compactly to form the rings after long incubation.

Short Aβ fragments form amyloid fibrils morphologically similar to those formed by full-length Aβ peptides. It would be interesting to study if short Aβ fragments can also form rings under the Aβ ring-forming conditions. Aβ16–22 is a well studied amyloidogenic fragment that readily forms fibrils around neutral pH. The peptide was dissolved in HFIP and studied using AFM after drying on mica (Figure 5). Panels A and B show the images recorded from freshly prepared 1 mM Aβ16–22 solution. The peptide forms short fibrous aggregates (panels A and B). Thin fibrils (~4–10 nm in thickness) are present as indicated by black arrows in panel A. Thick fibrils appear to arise from the lateral assembly of thinner fibrils as indicated by white arrows in panel A. Apart from the lateral assembly, the fibrils join their ends and give rise to ring-like structures having diameters ranging from 200 to 400 nm (panel A). Panel B also shows very small aggregates (≤5 nm thick) that are spread all over the mica surface. When imaging was performed on the 2-month-old 1 mM Aβ16–22 in HFIP, distinct ring-like structures are observed (panels C and D). The rings appear to form tubular structures through concentric stacking over each other as indicated by arrow in panel D. Panels E and F represent the images recorded from 2-month-old 1 mM Aβ16–22 in HFIP that was tenfold diluted prior to deposition on the mica. The images reveal that the ring-like structures are formed by fibrous aggregates that self-assemble into circular fashion, as also observed for the freshly dissolved peptide. Panel F clearly shows the stacking of two rings forming higher order structure, much like a tube. Short fibrous aggregates, not organized in the rings, are also observed.

Scanning Electron Microscopy (SEM) Imaging

SEM imaging of the aged peptides, Aβ40–43 (4-month old) and Aβ16–22 (2-month old) is shown in Figure 6. All the peptides form distinctive rings, albeit with different diameters. The diameters of the rings formed by Aβ40 and Aβ42 range from 200 to 400 nm (panels A and B, respectively). The rings formed by Aβ43 have thicker walls than those formed by Aβ40 and Aβ42, and their diameters are also much larger (panel C). Although small rings (<400 nm in diameter) are present (indicated by arrows in panel C), rings having diameters ~1 μm are also present. The diameters of the Aβ16–22 rings also vary but lie between 500 and1000 nm (panel D).

Circular Dichroism (CD) Spectroscopy

Secondary structures adopted by the peptides in HFIP (aged solutions) were studied using far-UV CD spectroscopy. The spectra recorded for the peptides are shown in Figure 7. Dotted line, dashed line, and dot–dash line represent the spectra recorded for 4-month-old Aβ40, Aβ42, and Aβ43, respectively. The peptides show a negative band ~203 nm and a shoulder ~220 nm. Qualitatively, the CD spectra suggest the presence of helix and unordered conformations. Secondary structural components were obtained for Aβ40–43 using CONTINLL program available in CDPro software

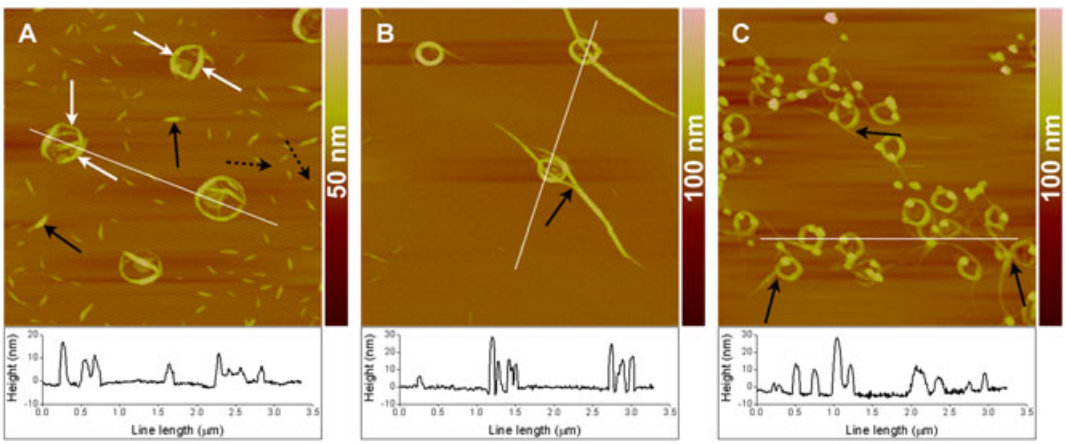

Figure 4. AFM images of 4-month-old Aβ peptides that were tenfold diluted in HFIP prior to drying on mica: (A) Aβ40; (B) Aβ42; and (C) Aβ43. Arrows are described in the AFM imaging section. Each panel is 4 μm × 4 μm in dimensions.

Journal of PeptideScience

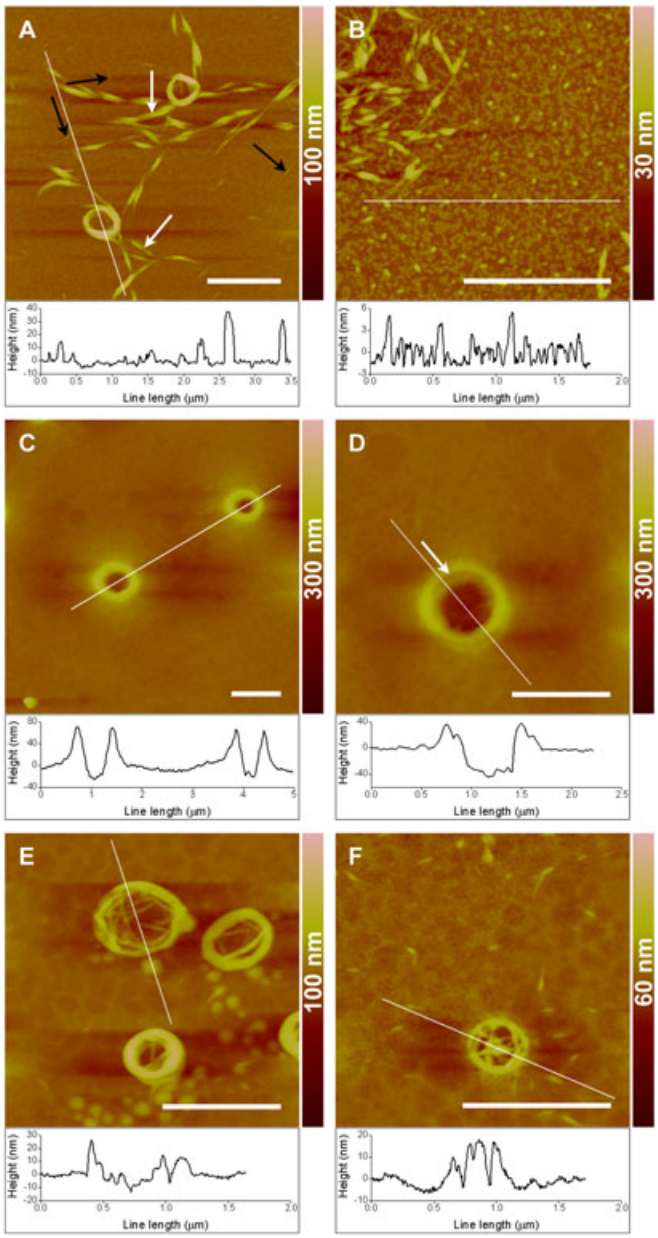

Figure 5. AFM images of 1 mM Aβ16–22 peptide; freshly dissolved (panels A and B), 2-month old (panels C and D), and 2-month old that was tenfold diluted in HFIP prior to drying on mica (panels E and F). Arrows are described in the AFM imaging section. Scale bars represent 1 μm.

package [29,30]. All the three peptides adopt an ensemble of β-structure, turns, and unordered conformations. Small fraction of α-helical conformation is also populated. Turn and unordered conformations constitute ~23% and 33% of the structures, respectively, in all the three peptides. In Aβ40 and Aβ43, ~11% α-helix and ~34% β-conformation were observed. Helical and β-conformations in Aβ42 constitute ~17% and 26% of the structures, respectively. Three-dimensional structures obtained for Aβ fibrils suggest that first 10–17 residues in the peptides are disordered [31–33], whereas residues 18–26 and 31–42 form two β-strands connected by the bend formed by ~5 residues [33]. This suggests that approximately one third of each peptide molecule is unstructured and ~50% of the molecule is in β-conformation. CD deconvolution using CONTINLL suggests that β-conformation and β-turns taken together constitute ~50% of the structures, whereas one third of the structure is unordered. The CD spectrum recorded for 2-month-old Aβ16–22 solution is shown by solid line. The peptide exhibits negative bands at ~226 nm and ~201 nm along with a positive band ~195 nm and a broad positive band spread around 210 nm. The band ~195 nm and the extended band ~210 nm arise from π-π* and n-π* transitions, respectively. These spectral characteristics have been suggested to arise from the β-structures, self-assembled through stacking of aromatic residues [34]. Similar CD spectra have been obtained for KLVFF in aqueous buffer and in TFE [35]. The CD deconvolution analysis was not performed on the Aβ16–22 spectrum as the spectrum has a large contribution from the phenylalanines present in the peptide. The method for analyzing the CD spectra makes use of the spectra of a set of reference proteins [29,30]. The spectra of the proteins in the set do not show significant aromatic contributions making the method unsuitable for the analysis of Aβ16–22 CD spectrum in HFIP.

Fourier Transform Infrared (FTIR) Spectroscopy

The rings observed using AFM and SEM microscopy were in dried state. Hence, it would be of interest to analyze the secondary structures adopted by the peptides in the dried form to correlate peptide structures with the self-assembled ring-like structures. The ATR-FTIR spectra recorded for the peptides dried from HFIP solutions are shown in Figure 8. Panels A, B, and C represent the spectra recorded from Aβ40, Aβ42, and Aβ43, respectively. The spectra were recorded for freshly dissolved (dotted lines) and aged peptide samples (solid lines). Amide I band, which is sensitive to secondary structures, is centered ~1659 cm^{-1} when spectra were recorded from freshly dissolved Aβ (dotted lines, panels A–C). The spectra suggest that the peptides adopt largely α-helical structure in the dried form [36]. Secondary structural components estimated using a linear least squares method with the program CDFIT indicated predominantly helical conformation for freshly dissolved Aβ40 and 42 in HFIP [15]. Spectra obtained after drying the 4-month-old Aβ solutions (solid lines) show amide I band centered ~1627 cm^{-1}, suggesting that the peptides adopt largely β-structure in the dried form. The spectra recorded for the peptides that were tenfold diluted in HFIP prior to performing ATR-FTIR studies did not show any significant change (data not shown). The rings obtained from Aβ are therefore composed of the peptides in β-conformation. The shoulder ~1664 cm^{-1} arises from disordered structures and β-turns and has been observed to some extent in the infrared spectra of other amyloids [37,38]. Presence of disordered and β-turn components is consistent with the three-dimensional structure suggested for Aβ fibrils [33]. These data suggest that drying after prolonged incubation of Aβ40–43 peptides in HFIP leads to structural transition from α-helical to β-conformation.

The amide I peaks for the Aβ16–22 peptide dried from freshly prepared and 2-month-old solutions are observed at 1630 cm^{-1} (dotted line) and 1627 cm^{-1} (solid line), respectively (panel D). These bands show that the peptide adopts β-structure in the dried form. The subtle differences in the spectra, however, can be attributed to the differences in the intermolecular hydrogen bond strengths [39–41] and some unassembled peptide present in the freshly dissolved peptide; long incubation results in characteristic 1627 cm^{-1} band observed for amyloid fibrils. Freshly dissolved Aβ11–28 peptide has been shown to adopt significant amount of β-structure [42]. Simulation studies have indicated that an α-helical intermediate is not necessary during Aβ16–22 self-assembly [43]. Unlike Aβ40–43, freshly dissolved Aβ16–22 adopts β-conformation

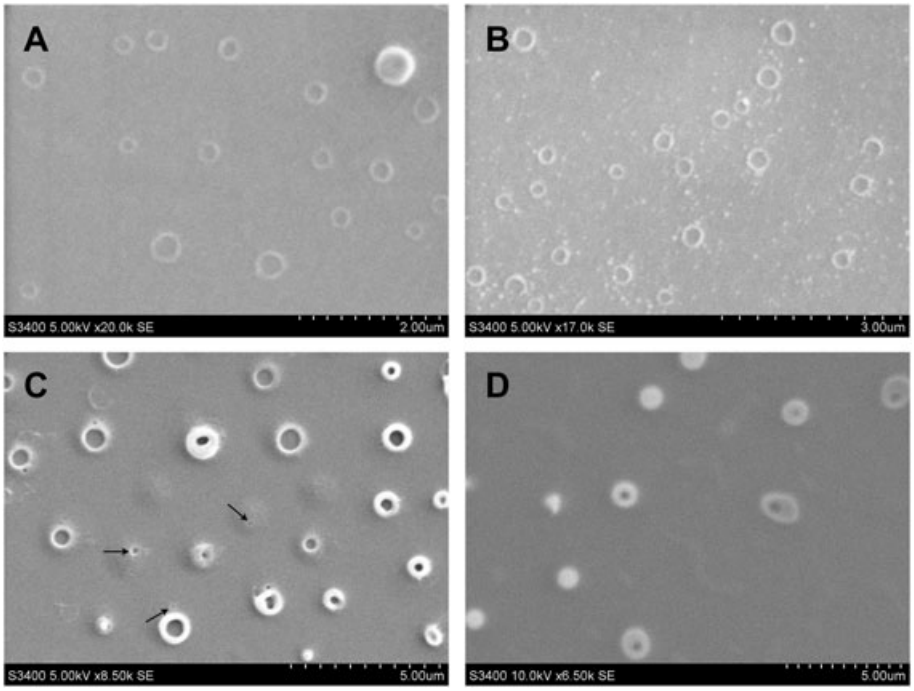

Figure 6. SEM images recorded from Aβ40 (panel A), Aβ42 (panel B), Aβ43 (panel C), and Aβ16–22 (panel D) after drying from aged peptide solutions in HFIP. Arrows are described in the SEM imaging section.

and shows ring-like structures (Figure 5A). The rings obtained from freshly dissolved Aβ40–43 are very thin and immature as compared with those obtained from 4-month-old solutions (Figures 1–4). This can be attributed to the secondary structures adopted by the peptides. The structural data from all the four peptides suggest that the peptides are in β-conformation in the self-assembled peptide nanostructures observed by AFM and SEM imaging.

Another interesting feature was observed after drying the freshly dissolved Aβ40–43 and redissolving in HFIP. When redissolved peptides were dried and studied using ATR-FTIR, a shoulder ~1632 cm^{-1} appears alongside the ~1658 cm^{-1}, band suggesting the population of β-structure on drying and redissolution (data not shown).

Thioflavin T (ThT) Fluorescence Imaging

As the peptides fold into β-conformation in the rings, it was of interest to examine if these structures cause enhancement in ThT fluorescence as observed with amyloid fibrils. ThT fluorescence assay for amyloid fibrils, however, is limited only to aqueous solutions. To determine whether the Aβ rings are amyloid in nature, we employed a modified ThT fluorescence imaging method as described in 'Materials and Methods' section. The images recorded are shown in Figure 9. Panels A, B, C, and D represent the images for Aβ40, Aβ42, Aβ43, and Aβ16-22, respectively. The rings formed by the peptides bind ThT and exhibit enhancement in its fluorescence. The β-conformation adopted by the peptides in dried form as well as their ability to bind and cause enhancement in ThT fluorescence suggests that the rings are amyloid-like in nature.

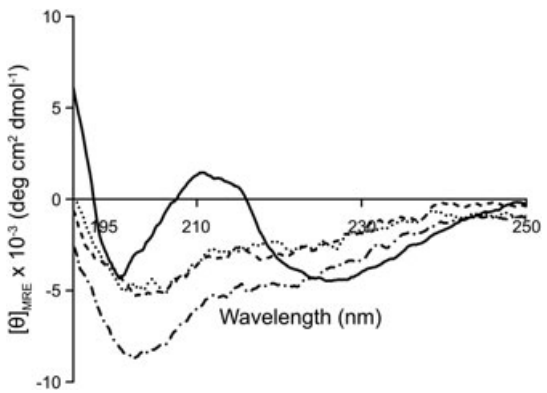

Figure 7. CD spectra recorded for Aβ40 (·····), Aβ42 (– – –), Aβ43 (· – · – · – ·), and Aβ16–22 (——) in HFIP.

Discussion

Aβ peptides deposit as insoluble fibrillar as well as nonfibrillar aggregates in the brains of Alzheimer's disease patients [44–46]. *In vitro* studies directed towards understanding Aβ self-assembly have also found a variety of aggregated species [12,26,27,47–50]. Early oligomers of Aβ are unstable and undergo conformational transition forming β-sheet rich assemblies [51]. Aβ and other amyloidogenic peptides are highly soluble in HFIP, and dissolution in HFIP has been used extensively to dissociate preformed aggregates of Aβ, its short fragments, and other amyloidogenic peptides [52–56]. Fluorinated alcohols have been shown to break β-sheet structure and induce α-helical conformations. Despite HFIP promoting helical conformation, extensive aggregation of Aβ in HFIP is observed as suggested by light scattering data [57]. HFIP enhances the rate of aggregation of Aβ at lower concentrations (~2% v/v) in aqueous solutions [58]. Involvement of α-helical to β-sheet structural transition as a key step in Aβ aggregation and insoluble fibril formation is well established [59–62]. The present study with Aβ40–43 and Aβ16–22 shows that HFIP induces formation of highly ordered self-assembled structures. The peptides form short fibrils that further assemble to form thicker fibrils and ring-like structures. The rings formed by Aβ43 are large

Journal of PeptideScience

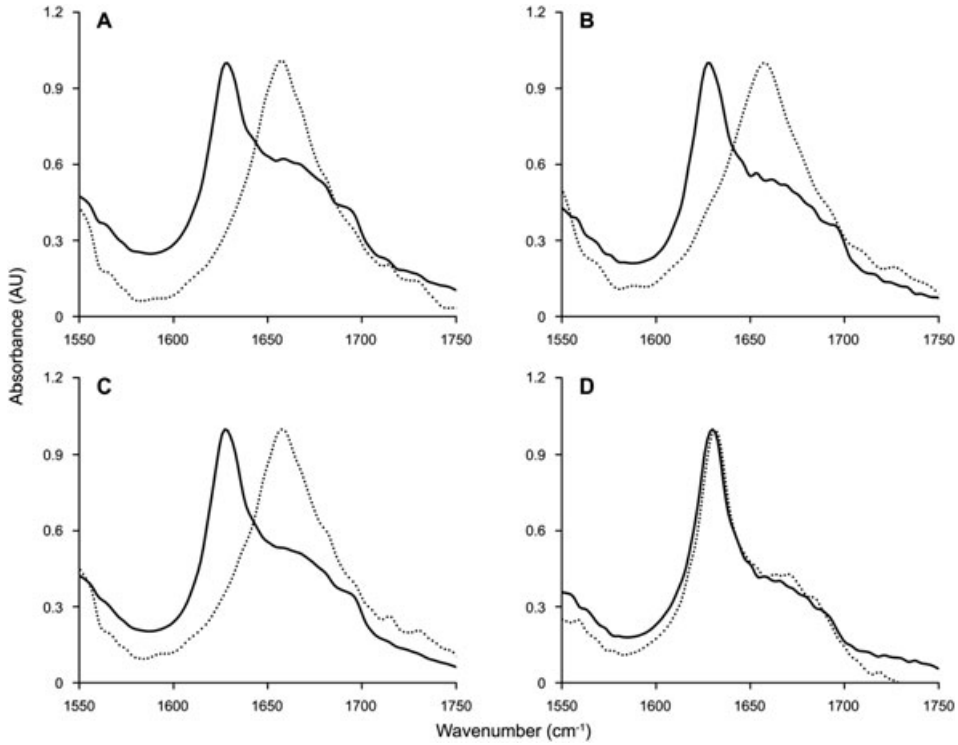

Figure 8. FTIR spectra after drying the freshly dissolved (·····) and aged (——) peptide solutions in HFIP: Aβ40 (panel A), Aβ42 (panel B), Aβ43 (panel C), and Aβ16–22 (panel D).

in diameter (up to ~1 μm), whereas those formed by Aβ40 and Aβ42 have smaller diameters (<600 nm). β-conformation adopted by the peptides in the self-assembled state, the thicknesses of these aggregates, and the enhancement caused in ThT fluorescence confirm amyloid fibril-like organization of the peptides in the rings. Aβ40 and Aβ42 are known to form ion channels in lipid bilayers [63]. AFM imaging of these channels reveals pores with 8–15 nm diameter that are formed by 4–6 globular subunits [64,65]. Similar pore-like annular structures have also been observed for mutant forms of Aβ, ABri and ADan as well as for α-synuclein, amylin, and Serum Amyloid A in lipid bilayers [66]. The pore-like structures formed by these proteins/peptides are less than 20 nm in diameter and elicit ion-channel currents [66]. The ring-like structures we have obtained from Aβ40–43 are very large structures wherein diameters range from ~150 nm to >1 μm depending on the peptide, and formation of these rings does not require lipid environment. The Aβ ion channels in lipid bilayer appear to be composed of globular subunits, whereas the rings obtained after drying from HFIP are composed of fibrillar structures. Large annular structures, similar to Aβ rings, have also been observed for amyloidogenic immunoglobulin light chain [67] and lysozyme [68] in aqueous solutions, short aromatic rich peptide in 50% aqueous methanol [69], and short peptides from human β_2-microglobulin and tau in HFIP [18,19]. Aβ16–22 has two phenylalanines and self-assembles through aromatic interactions in HFIP as suggested by its CD spectrum. The rings formed by the peptide might be similar to those formed by short aromatic rich peptides [18,69]. The rings observed for immunoglobulin light chain [67] are very similar to the Aβ rings with respect to their diameters and heights. Like Aβ rings, these rings are also associated with fibrillar aggregates, suggesting that the rings might arise by the circularization of fibrils. CD spectral analysis of the Aβ peptides suggests significant amount of β-conformation and turn-conformation. FTIR spectra of the aggregates show largely β-structure with small amount of turn conformation. This suggests that population of the β-conformation in the peptides drives their self-assembly. A recent molecular dynamics simulation study suggests β-barrel type organization of the ion channels formed by Aβ fragments [70]. The peptide molecules have been suggested

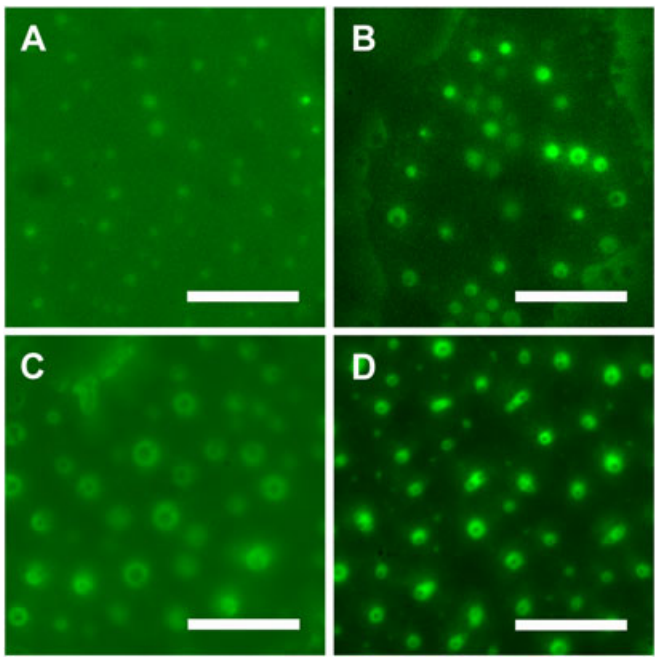

Figure 9. ThT fluorescence images of Aβ40 (panel A), Aβ42 (panel B), Aβ43 (panel C), and Aβ16–22 (panel D) after drying the aged solutions in HFIP. Scale bars represent 10 μm.

to adopt β-strand—turn—β-strand conformation and form parallel β-sheets. Such an arrangement suggests that linearization of these channels would give a structure very much similat to an Aβ protofilament. AFM imaging of Aβ rings obtained from HFIP suggests that the peptides form short fibrous structures as well as rings. Short fibrous aggregates range from very thin (~2 nm) to as thick as classical amyloid fibrils. Fibrous aggregates ~2 nm in diameter have been shown for Aβ42 by AFM and are suggested to be the single protofilament structures, i.e. structures with single cross-β unit [26–28]. Thicker fibers have tapering ends, suggesting that these structures might arise from stacking of thinner fibers. This lateral assembly would result in fibers with tapering ends if thinner filaments do not perfectly align along their lengths. This might also leave the ends of the fibers sticky, allowing them to join through their ends. AFM imaging suggests that the rings are composed of these fibrous aggregates that join through their ends to form longer fibrils and to enable bending that is required for formation of rings. The rings might have structural organization similar to that proposed for Aβ channels in membranes. The channels arise from globular subunits, whereas the rings appear to arise from the higher-order assembly of fibrous structures thereby having very large pore diameters. It is likely that the preformed fibrous structures are less amenable to bending thereby forming rings with large diameters. It is possible that the HFIP-induced ring-like amyloid structures differ from typical Aβ fibrils by their β-strand alignments or the registry of their β-sheets or hydrogen bonding which might be required to make the ends of the fibrils sticky.

Conclusion

The results in this study show that Aβ peptides dissolved in HFIP and rapidly dried, self-assemble into highly ordered ring-like structures. The peptide molecules fold into β-structure in these rings and cause enhancement in ThT fluorescence, suggesting that the molecular architecture of these rings is amyloid-like. HFIP has been used to obtain aggregate-free preparations of self-assembling peptides. Although our study pertains to Aβ peptides, it is possible that other amyloidogenic peptides also self-assemble into highly ordered structures when dissolved in HFIP. Hence, the use of HFIP for obtaining aggregate-free preparations of Aβ, its fragments, and other aggregating peptides needs to be reconsidered.

Acknowledgements

Funding from CSIR network project NWP035 is gratefully acknowledged. RN is the recipient of JC Bose Fellowship from the Department of Science and Technology, India.

References

1 Selkoe DJ. Translating cell biology into therapeutic advances in Alzheimer's disease. *Nature* 1999; **399**: A23-31.
2 LaFerla FM, Green KN, Oddo S. Intracellular amyloid-β in Alzheimer's disease. *Nat. Rev. Neurosci.* 2007; **8**: 499–509.
3 Woo HN, Baik SH, Park JS, Gwon AR, Yang S, Yun YK, Jo DG. Secretases as therapeutic targets for Alzheimer's disease. *Biochem. Biophys. Res. Commun.* 2011; **404**: 10–15.
4 Kuperstein I, Broersen K, Benilova I, Rozenski J, Jonckheere W, Debulpaep M, Vandersteen A, Segers-Nolten I, Van Der Werf K, Subramaniam V, Braeken D, Callewaert G, Bartic C, D'Hooge R, Martins IC, Rousseau F, Schymkowitz J, De Strooper B. Neurotoxicity of Alzheimer's disease Aβ peptides is induced by small changes in the Aβ42 to Aβ40 ratio. *EMBO J.* 2010; **29**: 3408–3420.
5 Welander H, Franberg J, Graff C, Sundstrom E, Winblad B, Tjernberg LO. Aβ43 is more frequent than Aβ40 in amyloid plaque cores from Alzheimer disease brains. *J. Neurochem.* 2009; **110**: 697–706.
6 Delacourte A, Sergeant N, Champain D, Wattez A, Maurage CA, Lebert F, Pasquier F, David JP. Nonoverlapping but synergetic tau and APP pathologies in sporadic Alzheimer's disease. *Neurology* 2002; **59**: 398–407.
7 Zagorski MG, Yang J, Shao H, Ma K, Zeng H, Hong A. Methodological and chemical factors affecting amyloid β peptide amyloidogenicity. *Methods Enzymol.* 1999; **309**: 189–204.
8 Sciarretta KL, Gordon DJ, Petkova AT, Tycko R, Meredith SC. Aβ40-Lactam(D23/K28) models a conformation highly favorable for nucleation of amyloid. *Biochemistry* 2005; **44**: 6003–6014.
9 Touchette JC, Williams LL, Ajit D, Gallazzi F, Nichols MR. Probing the amyloid-β(1–40) fibril environment with substituted tryptophan residues. *Arch. Biochem. Biophys.* 2010; **494**: 192–197.
10 Finder VH, Vodopivec I, Nitsch RM, Glockshuber R. The recombinant amyloid-β peptide Aβ1–42 aggregates faster and is more neurotoxic than synthetic Aβ1–42. *J. Mol. Biol.* 2010; **396**: 9–18.
11 Anguiano M, Nowak RJ, Lansbury PT Jr. Protofibrillar islet amyloid polypeptide permeabilizes synthetic vesicles by a pore-like mechanism that may be relevant to type II diabetes. *Biochemistry* 2002; **41**: 11338–11343.
12 Chromy BA, Nowak RJ, Lambert MP, Viola KL, Chang L, Velasco PT, Jones BW, Fernandez SJ, Lacor PN, Horowitz P, Finch CE, Krafft GA, Klein WL. Self-assembly of Aβ(1–42) into globular neurotoxins. *Biochemistry* 2003; **42**: 12749–12760.
13 Avidan-Shpalter C, Gazit E. The early stages of amyloid formation: biophysical and structural characterization of human calcitonin pre-fibrillar assemblies. *Amyloid* 2006; **13**: 216–225.
14 Anderson VL, Ramlall TF, Rospigliosi CC, Webb WW, Eliezer D. Identification of a helical intermediate in trifluoroethanol-induced alpha-synuclein aggregation. *Proc. Natl. Acad. Sci. U.S.A.* 2010; **107**: 18850–18855.
15 Stine WB Jr, Dahlgren KN, Krafft GA, LaDu MJ. In vitro characterization of conditions for amyloid-β peptide oligomerization and fibrillogenesis. *J. Biol. Chem.* 2003; **278**: 11612–11622.
16 Wood SJ, Maleeff B, Hart T, Wetzel R. Physical, morphological and functional differences between pH 5.8 and 7.4 aggregates of the Alzheimer's amyloid peptide Aβ. *J. Mol. Biol.* 1996; **256**: 870–877.
17 Dai X, Sun Y, Gao Z, Jiang Z. Copper enhances amyloid-β peptide neurotoxicity and non β-aggregation: a series of experiments conducted upon copper-bound and copper-free amyloid-β peptide. *J. Mol. Neurosci.* 2010; **41**: 66–73.
18 Chaudhary N, Singh S, Nagaraj R. Organic solvent mediated self-association of an amyloid forming peptide from β2-microglobulin: an atomic force microscopy study. *Biopolymers* 2008; **90**: 783–791.
19 Chaudhary N, Singh S, Nagaraj R. Morphology of self-assembled structures formed by short peptides from the amyloidogenic protein tau depends on the solvent in which the peptides are dissolved. *J. Pept. Sci.* 2009; **15**: 675–684.
20 Sanchez L, Madurga S, Pukala T, Vilaseca M, Lopez-Iglesias C, Robinson CV, Giralt E, Carulla N. Aβ40 and Aβ42 amyloid fibrils exhibit distinct molecular recycling properties. *J. Am. Chem. Soc.* 2011; **133**: 6505–6508.
21 Ban T, Morigaki K, Yagi H, Kawasaki T, Kobayashi A, Yuba S, Naiki H, Goto Y. Real-time and single fibril observation of the formation of amyloid β spherulitic structures. *J. Biol. Chem.* 2006; **281**: 33677–33683.
22 Exley C, House E, Collingwood JF, Davidson MR, Cannon D, Donald AM. Spherulites of amyloid-β42 in vitro and in Alzheimer's disease. *J. Alzheimers Dis.* 2010; **20**: 1159–1165.
23 Matsumura S, Shinoda K, Yamada M, Yokojima S, Inoue M, Ohnishi T, Shimada T, Kikuchi K, Masui D, Hashimoto S, Sato M, Ito A, Akioka M, Takagi S, Nakamura Y, Nemoto K, Hasegawa Y, Takamoto H, Inoue H, Nakamura S, Nabeshima Y, Teplow DB, Kinjo M, Hoshi M. Two distinct amyloid β-protein (Aβ) assembly pathways leading to oligomers and fibrils identified by combined fluorescence correlation spectroscopy, morphology, and toxicity analyses. *J. Biol. Chem.* 2011; **286**: 11555–11562.
24 Lu K, Jacob J, Thiyagarajan P, Conticello VP, Lynn DG. Exploiting amyloid fibril lamination for nanotube self-assembly. *J. Am. Chem. Soc.* 2003; **125**: 6391–6393.
25 Chaudhary N, Nagaraj R. Impact on the replacement of Phe by Trp in a short fragment of Aβ amyloid peptide on the formation of fibrils. *J. Pept. Sci.* 2011; **17**: 115–123.

26 Arimon M, Diez-Perez I, Kogan MJ, Durany N, Giralt E, Sanz F, Fernandez-Busquets X. Fine structure study of Aβ1-42 fibrillogenesis with atomic force microscopy. *FASEB J.* 2005; **19**: 1344–1346.
27 Mastrangelo IA, Ahmed M, Sato T, Liu W, Wang C, Hough P, Smith SO. High-resolution atomic force microscopy of soluble Aβ42 oligomers. *J. Mol. Biol.* 2006; **358**: 106–119.
28 Sato T, Kienlen-Campard P, Ahmed M, Liu W, Li H, Elliott JI, Aimoto S, Constantinescu SN, Octave JN, Smith SO. Inhibitors of amyloid toxicity based on β-sheet packing of Aβ40 and Aβ42. *Biochemistry* 2006; **45**: 5503–5516.
29 Sreerama N, Woody RW. Estimation of protein secondary structure from circular dichroism spectra: comparison of CONTIN, SELCON, and CDSSTR methods with an expanded reference set. *Anal. Biochem.* 2000; **287**: 252–260.
30 Sreerama N, Woody RW. On the analysis of membrane protein circular dichroism spectra. *Protein Sci.* 2004; **13**: 100–112.
31 Torok M, Milton S, Kayed R, Wu P, McIntire T, Glabe CG, Langen R. Structural and dynamic features of Alzheimer's Aβ peptide in amyloid fibrils studied by site-directed spin labeling. *J. Biol. Chem.* 2002; **277**: 40810–40815.
32 Petkova AT, Ishii Y, Balbach JJ, Antzutkin ON, Leapman RD, Delaglio F, Tycko R. A structural model for Alzheimer's β -amyloid fibrils based on experimental constraints from solid state NMR. *Proc. Natl. Acad. Sci. U.S.A.* 2002; **99**: 16742–16747.
33 Luhrs T, Ritter C, Adrian M, Riek-Loher D, Bohrmann B, Dobeli H, Schubert D, Riek R. 3D structure of Alzheimer's amyloid-β(1–42) fibrils. *Proc. Natl. Acad. Sci. U.S.A.* 2005; **102**: 17342–17347.
34 Gupta M, Bagaria A, Mishra A, Mathur P, Basu A, Ramakumar S, Chauhan VS. Self-assembly of a dipeptide- containing conformationally restricted dehydrophenylalanine residue to form ordered nanotubes. *Adv. Mater.* 2007; **19**: 858–861.
35 Krysmann MJ, Castelletto V, Kelarakis A, Hamley IW, Hule RA, Pochan DJ. Self-assembly and hydrogelation of an amyloid peptide fragment. *Biochemistry* 2008; **47**: 4597–4605.
36 Jackson M, Mantsch HH. The use and misuse of FTIR spectroscopy in the determination of protein structure. *Crit. Rev. Biochem. Mol. Biol.* 1995; **30**: 95–120.
37 Zurdo J, Guijarro JI, Dobson CM. Preparation and characterization of purified amyloid fibrils. *J. Am. Chem. Soc.* 2001; **123**: 8141–8142.
38 Andersen CB, Hicks MR, Vetri V, Vandahl B, Rahbek-Nielsen H, Thogersen H, Thogersen IB, Enghild JJ, Serpell LC, Rischel C, Otzen DE. Glucagon fibril polymorphism reflects differences in protofilament backbone structure. *J. Mol. Biol.* 2010; **397**: 932–946.
39 Haris PI, Chapman D. The conformational analysis of peptides using Fourier transform IR spectroscopy. *Biopolymers* 1995; **37**: 251–263.
40 Pelton JT, McLean LR. Spectroscopic methods for analysis of protein secondary structure. *Anal. Biochem.* 2000; **277**: 167–176.
41 Surewicz WK, Mantsch HH, Chapman D. Determination of protein secondary structure by Fourier transform infrared spectroscopy: a critical assessment. *Biochemistry* 1993; **32**: 389–394.
42 Juszczyk P, Kolodziejczyk AS, Grzonka Z. FTIR spectroscopic studies on aggregation process of the β-amyloid 11–28 fragment and its variants. *J. Pept. Sci.* 2009; **15**: 23–29.
43 Santini S, Wei G, Mousseau N, Derreumaux P. Pathway complexity of Alzheimer's β-amyloid Aβ16-22 peptide assembly. *Structure* 2004; **12**: 1245–1255.
44 Jakob-Roetne R, Jacobsen H. Alzheimer's disease: from pathology to therapeutic approaches. *Angew. Chem. Int. Ed Engl.* 2009; **48**: 3030–3059.
45 Kuo YM, Emmerling MR, Vigo-Pelfrey C, Kasunic TC, Kirkpatrick JB, Murdoch GH, Ball MJ, Roher AE. Water-soluble Aβ (N-40, N-42) oligomers in normal and Alzheimer disease brains. *J. Biol. Chem.* 1996; **271**: 4077–4081.
46 Haass C, Selkoe DJ. Soluble protein oligomers in neurodegeneration: lessons from the Alzheimer's amyloid β-peptide. *Nat. Rev. Mol. Cell Biol.* 2007; **8**: 101–112.
47 Goldsbury C, Frey P, Olivieri V, Aebi U, Muller SA. Multiple assembly pathways underlie amyloid-β fibril polymorphisms. *J. Mol. Biol.* 2005; **352**: 282–298.
48 Losic D, Martin LL, Mechler A, Aguilar MI, Small DH. High resolution scanning tunnelling microscopy of the β-amyloid protein (Aβ1-40) of Alzheimer's disease suggests a novel mechanism of oligomer assembly. *J. Struct. Biol.* 2006; **155**: 104–110.
49 Meinhardt J, Sachse C, Hortschansky P, Grigorieff N, Fandrich M. Aβ(1–40) fibril polymorphism implies diverse interaction patterns in amyloid fibrils. *J. Mol. Biol.* 2009; **386**: 869–877.
50 Ward RV, Jennings KH, Jepras R, Neville W, Owen DE, Hawkins J, Christie G, Davis JB, George A, Karran EH, Howlett DR. Fractionation and characterization of oligomeric, protofibrillar and fibrillar forms of β-amyloid peptide. *Biochem. J.* 2000; **348 Pt 1**: 137–144.
51 Cheon M, Chang I, Mohanty S, Luheshi LM, Dobson CM, Vendruscolo M, Favrin G. Structural reorganisation and potential toxicity of oligomeric species formed during the assembly of amyloid fibrils. *PLoS Comput. Biol.* 2007; **3**: 1727–1738.
52 Gordon DJ, Sciarretta KL, Meredith SC. Inhibition of β-amyloid(40) fibrillogenesis and disassembly of β-amyloid(40) fibrils by short β-amyloid congeners containing N-methyl amino acids at alternate residues. *Biochemistry* 2001; **40**: 8237–8245.
53 Green JD, Goldsbury C, Kistler J, Cooper GJ, Aebi U. Human amylin oligomer growth and fibril elongation define two distinct phases in amyloid formation. *J. Biol. Chem.* 2004; **279**: 12206–12212.
54 Lesne S, Koh MT, Kotilinek L, Kayed R, Glabe CG, Yang A, Gallagher M, Ashe KH. A specific amyloid-β protein assembly in the brain impairs memory. *Nature* 2006; **440**: 352–357.
55 Ryu J, Girigoswami K, Ha C, Ku SH, Park CB. Influence of multiple metal ions on β-amyloid aggregation and dissociation on a solid surface. *Biochemistry* 2008; **47**: 5328–5335.
56 Aileen Funke S, van Groen T, Kadish I, Bartnik D, Nagel-Steger L, Brener O, Sehl T, Batra-Safferling R, Moriscot C, Schoehn G, Horn AHC, Muller-Schiffmann A, Korth C, Sticht H, Willbold D. Oral treatment with the d-enantiomeric peptide D3 improves the pathology and behavior of Alzheimer's disease transgenic mice. *ACS Chem. Neurosci.* 2010; **1**: 639–648.
57 Fulop L, Zarandi M, Soos K, Penke B. Self-assembly of Alzheimer's disease-related amyloid peptides into highly ordered nanostructures. *Nanopages* 2006; **1**: 69–83.
58 Nichols MR, Moss MA, Reed DK, Cratic-McDaniel S, Hoh JH, Rosenberry TL. Amyloid-β protofibrils differ from amyloid-β aggregates induced in dilute hexafluoroisopropanol in stability and morphology. *J. Biol. Chem.* 2005; **280**: 2471–2480.
59 Walsh DM, Hartley DM, Kusumoto Y, Fezoui Y, Condron MM, Lomakin A, Benedek GB, Selkoe DJ, Teplow DB. Amyloid β-protein fibrillogenesis. Structure and biological activity of protofibrillar intermediates. *J. Biol. Chem.* 1999; **274**: 25945–25952.
60 Janek K, Rothemund S, Gast K, Beyermann M, Zipper J, Fabian H, Bienert M, Krause E. Study of the conformational transition of A β(1–42) using D-amino acid replacement analogues. *Biochemistry* 2001; **40**: 5457–5463.
61 Kirkitadze MD, Condron MM, Teplow DB. Identification and characterization of key kinetic intermediates in amyloid β-protein fibrillogenesis. *J. Mol. Biol.* 2001; **312**: 1103–1119.
62 Fezoui Y, Teplow DB. Kinetic studies of amyloid β-protein fibril assembly. Differential effects of alpha-helix stabilization. *J. Biol. Chem.* 2002; **277**: 36948–36954.
63 Arispe N, Pollard HB, Rojas E. Giant multilevel cation channels formed by Alzheimer disease amyloid β-protein [AβP-(1–40)] in bilayer membranes. *Proc. Natl. Acad. Sci. U.S.A.* 1993; **90**: 10573–10577.
64 Lin H, Bhatia R, Lal R. Amyloid β protein forms ion channels: implications for Alzheimer's disease pathophysiology. *FASEB J.* 2001; **15**: 2433–2444.
65 Lal R, Lin H, Quist AP. Amyloid beta ion channel: 3D structure and relevance to amyloid channel paradigm. *Biochim. Biophys. Acta* 2007; **1768**: 1966–1975.
66 Quist A, Doudevski I, Lin H, Azimova R, Ng D, Frangione B, Kagan B, Ghiso J, Lal R. Amyloid ion channels: a common structural link for protein-misfolding disease. *Proc. Natl. Acad. Sci. U.S.A.* 2005; **102**: 10427–10432.
67 Zhu M, Han S, Zhou F, Carter SA, Fink AL. Annular oligomeric amyloid intermediates observed by in situ atomic force microscopy. *J. Biol. Chem.* 2004; **279**: 24452–24459.
68 Malisauskas M, Zamotin V, Jass J, Noppe W, Dobson CM, Morozova-Roche LA. Amyloid protofilaments from the calcium-binding protein equine lysozyme: formation of ring and linear structures depends on pH and metal ion concentration. *J. Mol. Biol.* 2003; **330**: 879–890.
69 Joshi KB, Verma S. Sequence shuffle controls morphological consequences in a self-assembling tetrapeptide. *J. Pept. Sci.* 2008; **14**: 118–126.
70 Jang H, Arce FT, Ramachandran S, Capone R, Lal R, Nussinov R. β-Barrel topology of Alzheimer's β-amyloid ion channels. *J. Mol. Biol.* 2010; **404**: 917–934.

